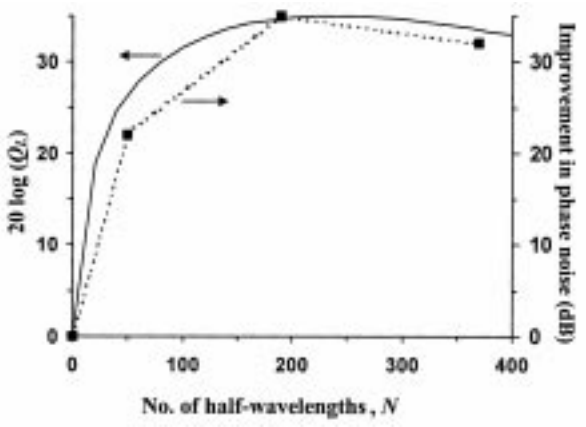

Fig. 5. Improvement in phase noise and $20\log(Q_L)$ versus N for the Ka-band oscillator.

TABLE II
MEASURED FREQUENCY PUSHING OF THE OSCILLATORS UNDER DIFFERENT RESONATOR TERMINATING CONDITIONS

Resonator terminating conditions	Frequency pushing of drain bias (MHz / V)	
	K-band oscillator	Ka-band oscillator
No resonator	217	295
Resonator R1	41	47
Resonator R2	13	26
Resonator R3	5	30

is obtained using resonator $R2$, with -90 dBc/Hz at 1-MHz offset. Increasing the resonator length to $R3$ actually causes 3-dB degradation in phase noise. Fig. 5 shows the measured phase noise improvement and the predicted increase in Q_L as a function of resonator length. The curve of $20\log(Q_L)$ predicts a maximum phase-noise improvement of 35 dB with resonator length of about 200 half-wavelengths. Beyond which, the associated line losses become increasing significant such that Q_L starts to decrease and phase noise degrades with increasing length. This trend is in agreement with the measured results.

In addition to phase-noise reduction, an increase in frequency stability was also observed with increasing resonator length. As an indication of frequency stability, frequency pushing of the two oscillators under different resonator terminating conditions is measured and given in Table II. With the addition of external resonators, a dramatic decrease in frequency pushing was observed for both oscillators.

V. CONCLUSION

This paper has demonstrated that oscillator frequency stabilization and phase-noise reduction can be achieved using simple transmission-line resonators. A simplified derivation of the improvement in phase noise has been verified through measured results of K- and Ka-bands monolithic oscillators. More than 20-dB improvement in phase noise was obtained for both oscillators. These results are obtained through the use of widely available coaxial cables, which may seem impracticably long. The actual length required, however, depend on the frequency of operation, loss characteristics, and dielectric constant of the transmission line. The wide availability of high-quality flexible low-loss cables, which can be compactly coiled, makes this technique a viable option for high-frequency applications. Therefore, the technique offers great potential in the development of low-cost MMIC oscillators with significantly improved noise performance.

ACKNOWLEDGMENT

The authors would like to thank Prof. C. Aitchison, University of Surrey, Guildford, Surrey, U.K., for many valuable discussions.

REFERENCES

[1] I. D. Robertson, Ed., *MMIC Design*. ser. IEE Circuits Syst. 7. London, U.K.: IEE, 1995, pp. 337–370.
[2] P. G. Wilson, "Monolithic 38 GHz dielectric resonator oscillator," in *IEEE Int. Microwave Symp. Dig.*, 1991, pp. 831–834.
[3] M. Funabashi *et al.*, "V-band AlGaAs/InGaAs heterojunction FET MMIC dielectric resonator circuit," in *IEEE GaAs IC Symp. Dig.*, 1994, pp. 30–33.
[4] M. Madihian and K. Honjo, "GaAs monolithic IC's for an X-band PLL-stabilized local source," *IEEE Trans. Microwave Theory Tech.*, vol. MTT-34, pp. 707–713, June 1986.
[5] A. Kanda, T. Hirota, H. Okaxaki, and M. Nakamae, "An MMIC chip set for V-band phase-locked local oscillator," in *IEEE GaAs IC Symp. Dig.*, 1995, pp. 259–262.
[6] K. K. M. Cheng and J. K. A. Everard, "Novel varactor tuned transmission line resonator," *Electron. Lett.*, vol. 25, no. 17, pp. 1164–1165, Aug. 1989.
[7] P. A. Rizzi, *Microwave Engineering*. Englewood Cliffs, NJ: Prentice-Hall, 1988, pp. 411–428.
[8] M. J. Underhill, "Fundamentals of oscillator performance," *Electron. Commun. Eng. J.*, vol. 44, pp. 185–193, Aug. 1992.
[9] K. S. Ang, M. J. Underhill, and I. D. Robertson, "Balanced monolithic oscillators at K- and Ka-band," *IEEE Trans. Microwave Theory Tech.*, vol. 48, pp. 187–193, Feb. 2000.
[10] D. B. Leeson, "A simple model of feedback oscillator noise spectrum," *Proc. IEEE*, vol. 54, pp. 329–330, Feb. 1966.

ALPS—A New Fast Frequency-Sweep Procedure for Microwave Devices

Din-Kow Sun, Jin-Fa Lee, and Zoltan Cendes

***Abstract*—The discretization of Maxwell equations results in a polynomial matrix equation in frequency. In this paper, we present a robust and efficient algorithm for solving the polynomial matrix equation. To solve this equation for a broad bandwidth, one previously performs a discrete frequency sweep where the resulting matrix needs to be inverted at numerous frequencies, while current procedure requires only one matrix inversion. Speed improvements compared to the discrete sweep range from 10 to 100 times, depending on number of resonance peaks encountered.**

***Index Terms*—Lanczos algorithm, Maxwell's equations, reduced-order system, transfinite-element method.**

I. INTRODUCTION

Over the last decade, tangential vector finite-element [1] and transfinite-element methods [2] have been developed for the solution of Maxwell equations. This discretization procedure results in a polynomial matrix equation in frequency. Especially in a waveguide structure, the modal fields of the ports depend strongly on frequency. To compute

Manuscript received October 11, 1999.

D.-K. Sun and Z. Cendes are with the Ansoft Corporation, Pittsburgh, PA 15219 USA.
J.-F. Lee is with the Electrical and Computer Engineering Department, Worcester Polytechnic Institute, Worcester, MA 01609 USA.

Publisher Item Identifier S 0018-9480(01)01087-0.

the response of a microwave device over a broad bandwidth, one originally performed a discrete frequency sweep where the resulting matrix equation is solved at numerous frequencies. This early procedure was very time consuming. In 1993, Yuan and Cendes [3] developed a fast frequency-sweep procedure requiring only one matrix inversion to compute the response over the entire band. This procedure is based on asymptotic waveform evaluation (AWE) [4], which evaluates a reduced-order model of the poles and zeros of the system transfer function by forming a Taylor series approximation of the response followed by Padé approximation. The technique is fast, but suffers inaccuracies since it was based on a power method that converges most strongly to the nearest mode. Due to the numerical instability of the AWE, Feldmann and Freund [5] presented a more reliable Lanczos procedure for solving a linear matrix equation in frequency. Later, Sun [6], [7] further proposed an adaptive Lanczos–Padé sweep (ALPS) to solve a polynomial matrix equation. An ALPS is a Lanczos type of procedure that solves only linear matrix equation in frequency. When an ALPS is applied to solve a polynomial matrix equation, it linearizes the equation at a couple of points and, therefore, it typically requires five time-consuming matrix solutions.

This paper begins by deriving the polynomial matrix equation using a transfinite-element method. Replacing the scattering matrix with a total scattering matrix, we not only reduce the number of right-hand-side vectors, but preserve a symmetric property for the scattering matrix over the entire band. However, property of energy conservation is exactly obeyed only at the expansion frequency. In Section III, we project this large dimensional matrix equation onto a much smaller dimensional one that can be solved discretely. We then discuss how one generates the projected vector set by block Lanczos iteration [8] such that the vector set contains all the eigenvectors of the interested band. With the computed locations of system poles, i.e., the eigenvalues of the matrix equation, one can knowingly select the frequency points to solve, and plot the frequency response curve without missing resonance peaks. The procedure is validated with some microwave structures in Section IV. This new ALPS procedure has been employed in the electromagnetics simulation package HFSS.

II. Transfinite-Element Formulation

The scattering problem of a typical four-port microstrip structure, as shown in Fig. 1, can be solved by applying transfinite-element formulation to the following dispersive vector wave equation:

$$\nabla \times \frac{1}{\mu_r} \nabla \times \vec{E} - k^2 \varepsilon_r(s) \vec{E} = 0 \tag{1}$$

where

$$s = \frac{\omega - \omega_o}{\omega_o} \qquad \varepsilon_r(s) = (s+1)\frac{\sigma}{j\omega_o\varepsilon_o} + (s+1)^2\varepsilon_r$$

and ω_o is the point of expansion. This gives rise to the following matrix equation:

$$\begin{bmatrix} Z_{II} & Z_{IP}M \\ M^T Z_{PI} & M^T Z_{PP} M + j\omega_o\mu_o(1+s)I \end{bmatrix} \begin{pmatrix} E_I \\ S \end{pmatrix} = \begin{pmatrix} -Z_{IP}M \\ -M^T Z_{PP} M + j\omega_o\mu_o(1+s)I \end{pmatrix} \tag{2}$$

where the subscripts I and P distinguish the unknown coefficients associated with the interior and port solutions, M is a matrix mapping interior solution on the ports to the modal coefficients, E_I is a multicolumn interior solution vector, and S is the generalized scattering matrix, respectively. The matrix entries are to be computed from a set of basis functions $\overline{\alpha}_i$

$$Z_{ij}(s) = \int \left(\nabla \times \overline{\alpha}_i \cdot \frac{1}{\mu_r} \nabla \times \overline{\alpha}_j - k^2 \overline{\alpha}_i \cdot \varepsilon_r(s) \overline{\alpha}_j \right) d\Omega. \tag{3}$$

Thorough derivation has been shown in [9]. It should be noticed that M is a strong function of s in the case of waveguide since the modal fields of the ports vary rapidly with frequency, as shown in Fig. 2. When approaching the cutoff frequency of waveguide, the field magnitude reaches infinity.

The right-hand side of (2) can be greatly simplified with a total scattering matrix $S' = I + S$ into

$$\begin{bmatrix} Z_{II} & Z_{IP}M \\ M^T Z_{PI} & M^T Z_{PP} M + j\omega_o\mu_o(1+s)I \end{bmatrix} \begin{pmatrix} E_I \\ S' \end{pmatrix} = 2j\omega_o\mu_o(1+s) \begin{pmatrix} 0 \\ I \end{pmatrix}. \tag{4}$$

Since the frequency dependency of the right-hand-side vectors is factorized, computational time is considerably reduced.

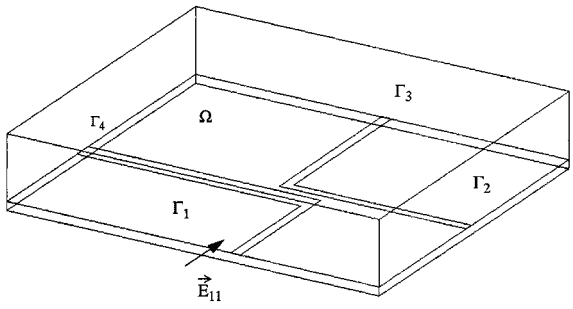

Fig. 1. Four-port microstrip structure.

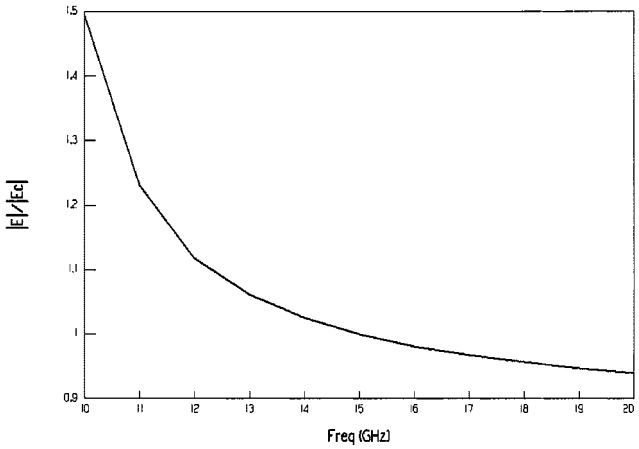

Fig. 2. Field dispersion of a rectangular waveguide of dimensions of 8×16 mm^2. $|Ec|$ is the field strength at 15 GHz.

III. New ALPS

A. Formulation

Equation (4) can be approximated by the following polynomial matrix equation:

$$\left(A_o - \sum_{i=1}^{n_A} s^i A_i \right) x(s) = b(s) \tag{5}$$

where n_A is determined by bounding the difference between (4) and (5). Testing (5) with a vector set $V = \{v_1, v_2, \ldots, v_{n_v}\}$ and looking for a solution $x(s) = V\overline{x}(s)$ gives

$$\left(H_o - \sum_{i=1}^{n_A} s^i H_i\right)\overline{x}(s) = V^T b(s) \tag{6}$$

where $H_k = V^T A_k V$, $k = 0, \ldots, n_A$. Therefore, the solution of (5) is

$$x(s) = V \frac{1}{\left(H_o - \sum_{i=1}^{n_A} s^i H_i\right)} V^T b(s). \tag{7}$$

The dimension of (7), i.e., n_V, is small enough to be solved with the Gaussian solver to perform a discrete sweep.

The S-matrix that we are interested in is

$$S(s) = 2(1+s)\gamma e^T V \frac{1}{\left(H_o - \sum_{i=1}^{n_A} s^i H_i\right)} V^T e - I \tag{8}$$

where $e^T = [0\ I]$ and $\gamma = j\omega_0\mu_0$. Notice that $S(s) = S^T(s)$. At the point of expansion $s = 0$, $\overline{x} = (1, 0, 0 \ldots 0)^T$, $x = A_o^{-1}b(0)$ and, therefore, the solution is exact.

The following theorem can be proven for the transfinite-element method.

Theorem 1: For a lossless system, the S-matrix computed directly from (2) obeys the property of energy conservation, i.e., $SS^* = I$.

Proof: Equation (2) can be solved by

$$S = (Y + \gamma(1+s)I)^{-1}(-Y + \gamma(1+s)I)$$

where

$$Y = M^T Z_{PP} M - M^T Z_{PI} Z_{II}^{-1} Z_{IP} M.$$

For a lossless system, Z is real and, thus, so is Y, i.e., $Y = Y^*$. Thus,

$$SS^* = \Big(Y + \gamma(1+s)I\Big)^{-1}\Big(-Y + \gamma(1+s)I\Big) \cdot\Big(Y - \gamma(1+s)I\Big)^{-1}\Big(-Y - \gamma(1+s)I\Big) = I.$$

In theory, the ALPS solution satisfies the property only at the expansion frequency, but our numerical results obey it fairly well over the entire band.

B. Procedure

The entire procedure consisting of computing the polynomial matrix equation, generating the vector set, and solving the matrix equation of smaller dimension is listed in the following steps.

- Step 1) Compute the frequency dependency of the matrix entries. This is done by adaptively adding more points until enough frequency points are chosen to provide a good approximation [10]. Step 1 gives you n_A and (5).
- Step 2) Start with $\binom{0}{I}$ to generate V for the (A_o, A_1) pair by block Lanczos iteration with selective orthogonalization [11]. If the selective orthogonalization is not employed, the Lanczos iteration will eventually fail. Using the facts that $A_i \cong 0$ when $i \geq 3$ and $A_2 \cong 0.5A_1$, one can estimate the poles of (5), i.e., p, from the computed eigenvalues of (A_o, A_1), λ by the following relationship:

$$p = -1 + \sqrt{1 + 2\lambda}. \tag{9}$$

Since the poles converge more or less sequentially according to its distance from the expansion frequency on the complex plane, one can terminate the procedure if the latest converged pole is located outside the circle covering the interested band with the center of circle at the expansion frequency, or one can plug the solution back to (5) to compute the residues for the entire band, and examine it if a good solution is reached.

- Step 3) Compute H_i's.
- Step 4) To compute $S(s)$, solve (6) directly according to the locations of the estimated poles. If the poles are close to the real axis, we need to compute many points around the poles.

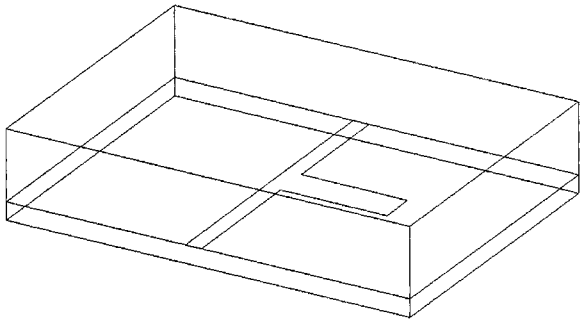

Fig. 3. Microstrip T-junction.

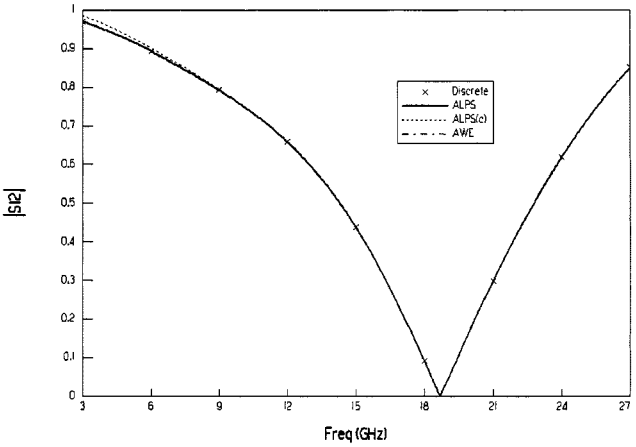

Fig. 4. Comparison of scattering parameters for Fig. 3. ALPS(c) is the ALPS solution neglecting the dispersion of the port solution.

IV. Numerical Results

Since the numerical solution of the discrete sweep of (2) is the exact solution of the fast sweep, we shall compare ALPS results with this results. The first geometry, shown in Fig. 3, is a microstrip T-junction, where the infinitively thin microstrip is 0.23-mm wide, the stub is 0.51-mm wide and 1.53-mm long, the substrate is 0.254-mm thick, and the relative dielectric constant of the substrate is 9.9. This problem is solved with both the ALPS and AWE methods. As shown in Fig. 4, the numerical results of both methods are indistinguishable, and both agree with the discrete sweep. The fields of the quasi-TEM mode of the microstrip ports are almost constant, i.e., nondispersive, throughout the frequency band. Therefore, using the modal solutions of the expansion frequency of 15 GHz for the entire band to compute an ALPS solution fairs quite well.

To demonstrate the importance of modeling the dispersion of the port correctly, we use a rectangular waveguide with dimensions of 8×16 mm^2 as an example. We have first employed fifth-order polynomials

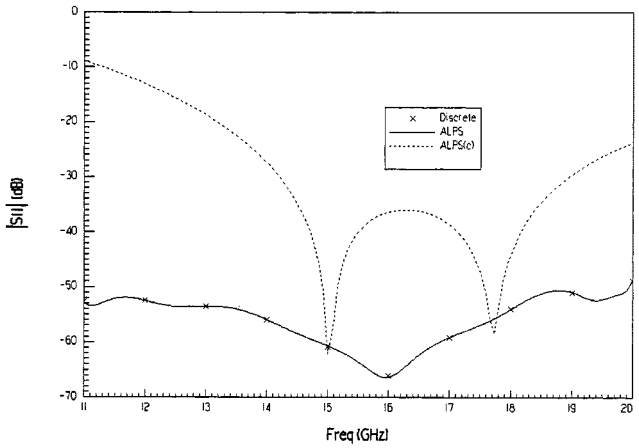

Fig. 5. Effect of neglecting the dispersion of the port solution for a rectangular waveguide of dimensions of 8×16 mm^2. ALPS(c) is the ALPS solution neglecting the dispersion of the port solution.

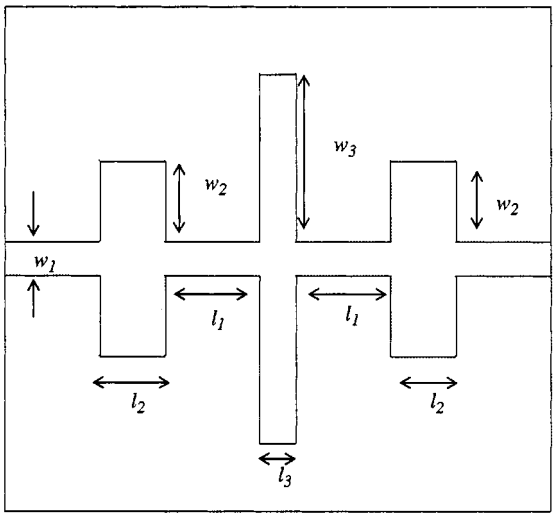

Fig. 6. Top view of a microstrip low-pass filter. $w1 = 25$ mil, $w2 = 60$ mil, $w3 = 125$ mil, $\ell 1 = 65$ mil, $\ell 2 = 45$ mil, and $\ell 3 = 25$ mil.

to interpolate the modal solutions of the ports. This problem is solved with the ALPS method. Again, the agreement with the discrete sweep is excellent, as shown in Fig. 5. We then assume the modal solutions are constant throughout the whole band. By using the modal solutions of 15 GHz, the numerical results display larger discrepancy away from 15 GHz.

To test the reliability of the ALPS, we consider a microstrip low-pass filter. The top view of the filter is depicted in Fig. 6. The substrate is 25-mil thick, and has a relative dielectric constant of 9.6. Due to the presence of three stubs, the spectral response curve of this filter from 2 to 20 GHz has three poles. It is suspected that picking the expansion frequency too close to one of the poles may have significant impacts on the accuracy of other two poles. Therefore, in Fig. 7, we move the point of expansion to reveal its effect on the AWE and ALPS solutions. If the point of expansion is chosen away from the poles at 12 GHz, both methods produce reasonable solutions. However, as in Fig. 8, if the point of expansion is close to one of the poles, the AWE completely misses the other two poles, while the ALPS unaffectedly maintains its accuracy throughout the whole band.

The last problem is a waveguide transition from 4×6 to 8×16 mm^2 guides, shown in Fig. 9. Initially, we compute the ALPS solution with a single propagating mode. In Fig. 10, the ALPS shows a couple of

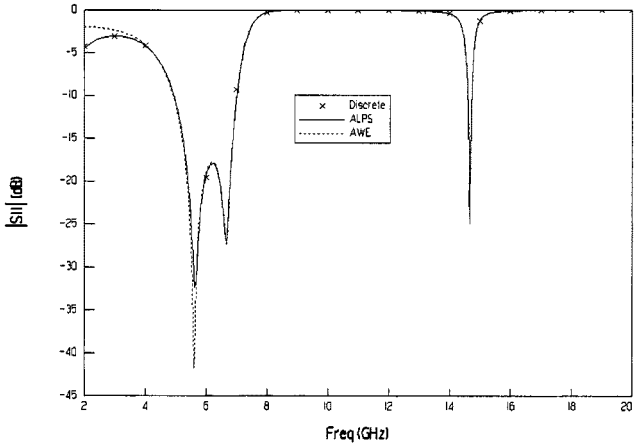

Fig. 7. Comparison of scattering parameters for Fig. 6. The point of expansion is 12 GHz.

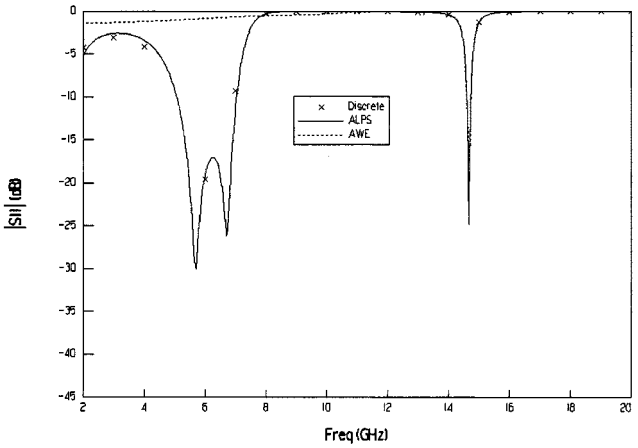

Fig. 8. Effect of shifting the point of expansion for Fig. 6. The point of expansion is 15 GHz.

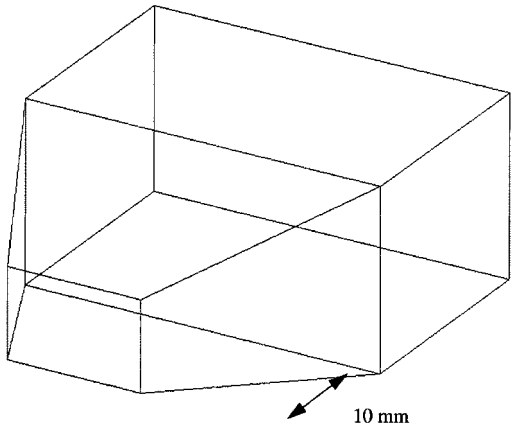

Fig. 9. Waveguide transition from 4×6 to 8×16 mm^2 guides.

spurious resonance peaks in the band. We discover that, at this frequency, the larger guide is able to support eight propagating modes. Since we have only permitted ground-mode propagation in the numerical simulation, the higher modes generated by waveguide discontinuity are trapped in the cavity, producing the resonance peaks. After rerunning the problem with eight propagating modes, the peaks disappear, while the rest of response curve is little affected. Without a reliable frequency-sweep procedure, we can hardly catch the spurious

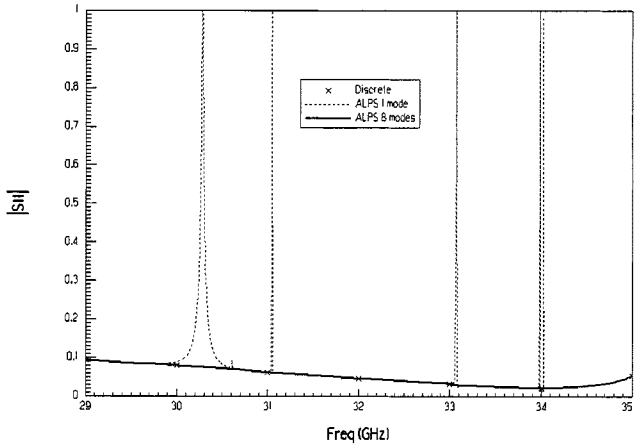

Fig. 10. Effect of not including all the propagating modes for Fig. 9.

peaks and, hence, realize the importance of including all the propagating modes when using the transfinite-element method.

Compared to the AWE, although the ALPS spends extra time on computing the eigenvectors of a tridiagonal matrix, it is not only more reliable, but overall more efficient, because it can tell the range of validity and, hence, terminate at earlier time. Its computational time depends on the number of poles inside the circle of convergence covering the interested band. Typically, four projecting vectors per pole are needed. The poles near the real axis influences the frequency response curve the most. It is unwise to ask for too big a frequency range because this will enclose a lot of unimportant poles in the circle of convergence. It is more efficient to break up a large band into a series of smaller bands. Since each band requires its own matrix inversion, this cost has to be balanced against the saving on the number of projecting vectors needed. When the sparse matrix decomposition is replaced by an iterative solver, the strategy will tilt toward more finer subdivisions of the band.

The limitation of current procedure lies on the assumption that higher order matrices of the polynomial matrix equation are relatively small. In the case of high lossy problem, the entries of higher order matrices may not be small. Numerical experiments show the procedure takes more iterations to converge. Also, (9) is no longer an appropriate approximation of system eigenvalues. One must compute the eigenvalues of the reduced system.

ACKNOWLEDGMENT

The authors would like to thank their colleague, Dr. R. Dyczij-Edlinger, Ansoft Corporation, Pittsburgh, PA, for his ingenious insight.

REFERENCES

[1] J. C. Nedelec, "Mixed finite elements in R3," *Numer. Math.*, vol. 35, pp. 315–341, 1980.
[2] Z. Cendes and J.-F. Lee, "The transfinite element method for modeling MMIC devices," *IEEE Trans. Microwave Theory Tech.*, vol. 36, pp. 1639–1649, Dec. 1988.
[3] X. Yuan and Z. Cendes, "A fast method for computing the spectral response of microwave devices over a broad bandwidth," in *Proc. IEEE AP-S/URSI Int. Symp. Dig.*, Ann Arbor, MI, June 1993, p. 196.
[4] L. T. Pillage and R. A. Rohrer, "Asymptotic waveform evaluation for timing analysis," *IEEE Trans. Computer-Aided Design*, vol. 9, pp. 352–366, Apr. 1990.
[5] P. Feldmann and R. W. Freund, "Efficient linear circuit analysis by Padé approximation via the Lanczos process," *IEEE Trans. Computer-Aided Design*, vol. 14, pp. 639–649, May 1995.
[6] D.-K. Sun, "ALPS—An adaptive Lanczos-Padé spectral solution of mixed-potential integral equation," in *USNC/URSI Radio Sci. Meeting Dig.*, July 1996, p. 30.
[7] D.-K. Sun, "ALPS—An adaptive Lanczos–Padé spectral solution of mixed-potential integral equation," *Comput. Methods Appl. Mech. Eng.*, vol. 169, pp. 425–432, 1999.
[8] C. Lanczos, "An iterative method for the solution of the eigenvalue problem of linear differential and integral operators," *J. Res. Natl. Bur. Stand.*, vol. 45, pp. 255–282, 1950.
[9] J. E. Bracken, D.-K. Sun, and Z. Cendes, "S-domain methods for simultaneous time and frequency characterization of electromagnetic devices," *IEEE Trans. Microwave Theory Tech.*, vol. 47, pp. 1277–1290, Sept. 1998.
[10] E. H. Newman, "Generation of wide-band data from the method of moments by interpolating the impedance matrix," *IEEE Antennas Propagat.*, vol. 30, pp. 1820–1824, Dec. 1988.
[11] B. N. Parlett and D. S. Scott, "The Lanczos algorithm with selective orthogonalization," *Math. Comput.*, vol. 33, no. 145, pp. 217–238, 1979.

Analysis and Design of Impedance-Transforming Planar Marchand Baluns

Kian Sen Ang and Ian D. Robertson

***Abstract*—A technique for designing impedance-transforming baluns is presented in this paper. It is based on the Marchand balun with two identical coupled lines. By varying the coupling factor of the coupled sections, a wide range of impedance transforming ratios can be achieved. In addition, a resistive network added between the balun outputs is proposed to achieve balun output matching and isolation. Microstrip baluns, matched at all ports, for transforming from a 50-Ω source impedance to 40-Ω as well as 160-Ω load terminations are realized to demonstrate the technique.**

***Index Terms*—Baluns, circuit analysis, couplers, impedance matching.**

I. INTRODUCTION

Baluns are key components in balanced circuit topologies such as double balanced mixers, push–pull amplifiers, and frequency doublers [1]–[3]. Various balun configurations have been reported for applications in microwave integrated circuits (MICs) and microwave monolithic integrated circuits (MMICs) [1]–[8]. Among them, the planar version of the Marchand balun [9] is perhaps one of the most attractive due to its planar structure and wide-band performance.

The planar Marchand balun consists of two coupled sections, which may be realized using microstrip coupled lines [5], Lange couplers [6], multilayer coupled structures [7], or spiral coils [8]. These baluns are usually designed through circuit simulations using full-wave electromagnetic analysis [1] or lumped-element models [8]. Various synthesis techniques using coupled-line equivalent-circuit models and analytically derived scattering parameters have also been reported [10], [11]. In this paper, the planar Marchand balun is analyzed as a combination

Manuscript received November 23, 1999. This work was supported by the Engineering and Physical Sciences Research Council. The work of K. S. Ang was supported by the Defence Science Organization National Laboratories.

The authors are with the Microwave and Systems Research Group, School of Electronic Engineering, Information Technology and Mathematics, University of Surrey, Guildford, Surrey GU2 7XH, U.K. (e-mail: k.ang@eim.surrey.ac.uk).

Publisher Item Identifier S 0018-9480(01)01088-2.